LETTERS

Discovery of a magma chamber and faults beneath a Mid-Atlantic Ridge hydrothermal field

Satish C. Singh[1], Wayne C. Crawford[1], Hélène Carton[1], Tim Seher[1], Violaine Combier[1], Mathilde Cannat[1], Juan Pablo Canales[2], Doga Düsünür[1], Javier Escartin[1] & J. Miguel Miranda[3]

Crust at slow-spreading ridges is formed by a combination of magmatic and tectonic processes, with magmatic accretion possibly involving short-lived crustal magma chambers[1]. The reflections of seismic waves from crustal magma chambers have been observed beneath intermediate[2,3] and fast-spreading centres[4,5], but it has been difficult to image such magma chambers beneath slow-spreading centres[6,7], owing to rough seafloor topography and associated seafloor scattering[7,8]. In the absence of any images of magma chambers[6] or of subsurface near-axis faults, it has been difficult to characterize the interplay of magmatic and tectonic processes in crustal accretion and hydrothermal circulation at slow-spreading ridges. Here we report the presence of a crustal magma chamber beneath the slow-spreading Lucky Strike segment of the Mid-Atlantic Ridge. The reflection from the top of the magma chamber, centred beneath the Lucky Strike volcano and hydrothermal field, is approximately 3 km beneath the sea floor, 3–4 km wide and extends up to 7 km along-axis. We suggest that this magma chamber provides the heat for the active hydrothermal vent field above it. We also observe axial valley bounding faults that seem to penetrate down to the magma chamber depth as well as a set of inward-dipping faults cutting through the volcanic edifice, suggesting continuous interactions between tectonic and magmatic processes.

These results come from a recent (June–July 2005) seismic reflection survey over the Lucky Strike volcano and hydrothermal vent field (Fig. 1) made from the French RV *l'Atalante*. The Lucky Strike volcano is situated at the centre of the Lucky Strike segment of the Mid-Atlantic Ridge (MAR), which spreads at 22 mm yr^{-1} (ref. 9). Although the large-scale topography[9] and basalt geochemistry[10] indicate that the Lucky Strike segment might be influenced by the Azores hotspot[11], the morphological and tectonic architecture of the Lucky Strike segment has many of the characteristics of a slow-spreading ridge[12]. A well-developed and fault-bounded axial valley is ~15–20 km wide and deepens from ~1,600 m at the volcano summit to >4,000 m near the segment ends; beyond the rift walls the seafloor morphology is dominated by fault-controlled abyssal hills[12]. A seismic swarm within the segment was detected in 2001 by a regional hydrophone network and might have been caused by melt movement (dyking) in the crust[13].

The Lucky Strike volcano is one of the largest central volcanoes along the MAR axis, indicating enhanced melt supply to the segment centre. It is about 6 km wide and 15 km long, and has a relatively smooth topography[14]. Gravity data suggest that the crust should be thick beneath the volcano[9,12]. High-resolution bathymetry data show two major ridge-parallel faults cutting through the volcanic edifice and defining a recent axial graben (rift)[15]. The summit of the volcano hosts one of the largest hydrothermal fields at the MAR (>1 km^2),

having numerous vents with outflow temperatures of up to 324 °C (ref. 16), and supporting a hydrothermal ecosystem[17]. The Lucky Strike segment is one of the sites chosen by the scientific community for long-term seafloor observation to study the interaction between magmatic, tectonic, hydrothermal, and biological processes at mid-ocean ridges.
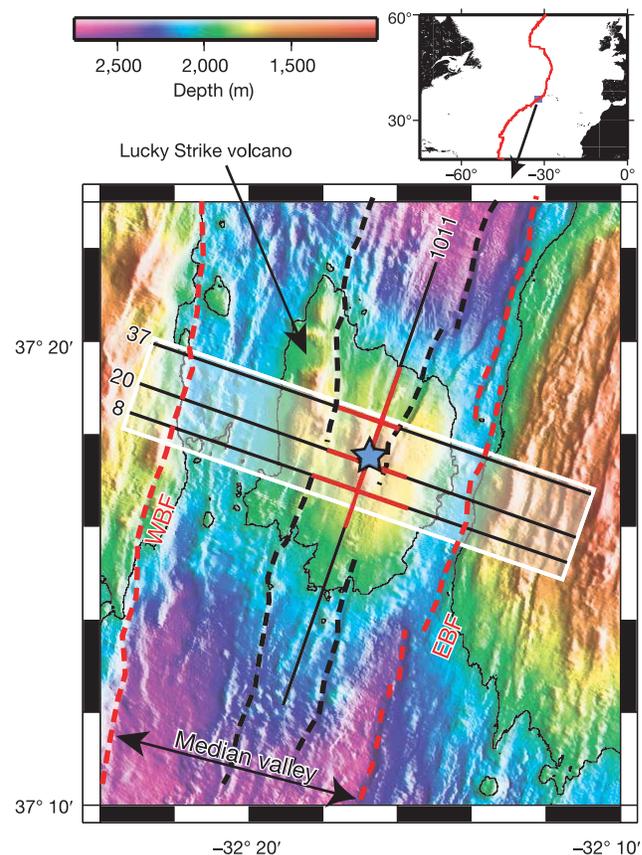

Figure 1 | Lucky Strike seismic survey location. Bathymetric map of Lucky Strike volcano and median rift valley. The black contour is at 2,000 m water depth and the blue star marks the Lucky Strike hydrothermal field. Red dashed curves mark the median valley bounding faults (WBF and EBF) and black dashed curves mark the recent graben (new rift) bounding faults. The white rectangle marks the bounds of the three-dimensional seismic reflection survey area, black lines show the seismic lines (8, 20, 37, 1011) used in this study and red lines show the locations of the observed AMC along these lines (Fig. 2). Inset, the MAR is marked in red.

[1]Laboratoire de Géosciences Marines, Institut de Physique du Globe de Paris, 4 Place Jussieu, 75252 Paris, France. [2]Department of Geology and Geophysics, Woods Hole Oceanographic Institution, 360 Woods Hole Road, Woods Hole, Massachusetts 02543, USA. [3]Centro de Geofísica, University of Lisbon, Campo Grande, Ed C8, 1749-016 Lisbon, Portugal.

Figure 2 shows images from four seismic reflection lines over the centre of the volcano. The southern line 8, over the flattest part of the volcano, shows a 4-km-wide reflection event at ~1.3 s below the sea floor. The polarity of this reflection is the reverse of that of the sea floor and layer 2A reflections (Fig. 3a), suggesting that it is produced by a negative velocity contrast. We suggest that this is an axial magma chamber (AMC) reflection. If we assume an average velocity of 5 km s^{-1} in the upper crust, then this reflector lies 3.25 km below the sea floor. We also observe a layer 2A reflection at about 0.5 s below the sea floor (1 km depth for an assumed velocity of 4 km s^{-1}). We notice reflection events that dip towards the centre of the ridge and are roughly aligned with the axial valley bounding fault-line scarps observed on the sea floor, which we interpret as rift bounding faults (East Bounding Fault (EBF) and West Bounding Fault (WBF), Fig. 2). Smaller faults that bound the graben within the rift valley floor are also visible in the proximity of the Lucky Strike hydrothermal field, and reach the base of layer 2A. To visualize the geometry of the faults in the crust, we remove the seafloor effect by flattening the seismic image using a smooth seafloor topo-graphy (Supplementary Fig. S1), which clearly shows that these faults arrive at the sea floor. The event on the eastern side (EBF) is strong and can be observed on common mid-point data (gather) (Fig. 3c). If we assume an average velocity of 5 km s^{-1}, the fault dip is 45–50°, consistent with dips determined from earthquake fault plane solutions at slow-spreading ridges[18]. The event seems to continue 0.6 s below the AMC, but this could be an imaging effect that may disappear after migration. However, we can confidently say that the EBF goes down to at least the AMC depth. The event on the western side (WBF) has a shallower dip and does not appear to continue below the AMC (Fig. 2). We also observe a steep event (50°) on the western flank of the volcano that terminates above the AMC. This event is associated with the western fault bounding the graben on top of the volcano.

Line 20 crosses the centre of the volcano, where the hydrothermal vents are observed. Layer 2A is slightly thicker (0.55 s) and the AMC is slightly narrower (3.5 km) than those along line 8. The dipping events interpreted as faults are also present on this line. The hydrothermal field lies around small inward-dipping faults that go down to the bottom of layer 2A. Line 37 traverses the northern, rifted part of the volcano. The layer 2A is thinnest (0.5 s) beneath the graben floor and thickest (0.65 s) beneath the volcanic ridge. The AMC appears to narrow northward from 4 km to 2.5 km over a distance of 2.8 km. A well-imaged westward-dipping event, inter-preted as a fault, penetrates downward from the eastern graben wall.

Line 1011 is an along-axis profile that extends over the entire volcanic edifice (Figs 1 and 2). The layer-2A reflection lies about 0.5 s below the sea floor, except beneath the volcano where it is slightly thicker (0.65 s). The AMC is observed for about 7 km along the axis. We also observe several subhorizontal features below layer 2A, which could be caused by frozen melt sills or ridge-parallel faults, such as the graben bounding faults.

The presence of an AMC has been reported along the Reykjanes ridge using seismic reflection and refraction data[8]. Although the Reykjanes ridge is a part of the MAR, it lacks slow-spreading-ridge characteristics and has been influenced by the nearby Iceland hot-spot. A small AMC reflection was also reported beneath the Snake Pit hydrothermal field at the MAR, but the quality of the image is poor[19]. Seismic tomography results have shown the presence of low velocities in the lower crust indicative of high temperatures and partial melt[20], but no AMC reflections were observed.

The observation of a large AMC at crustal depths beneath the Lucky Strike segment has important consequences for our understanding of magmatic-tectonic interactions at slow-spreading ridges. Figure 4 shows a schematic diagram summarizing the three-dimensional
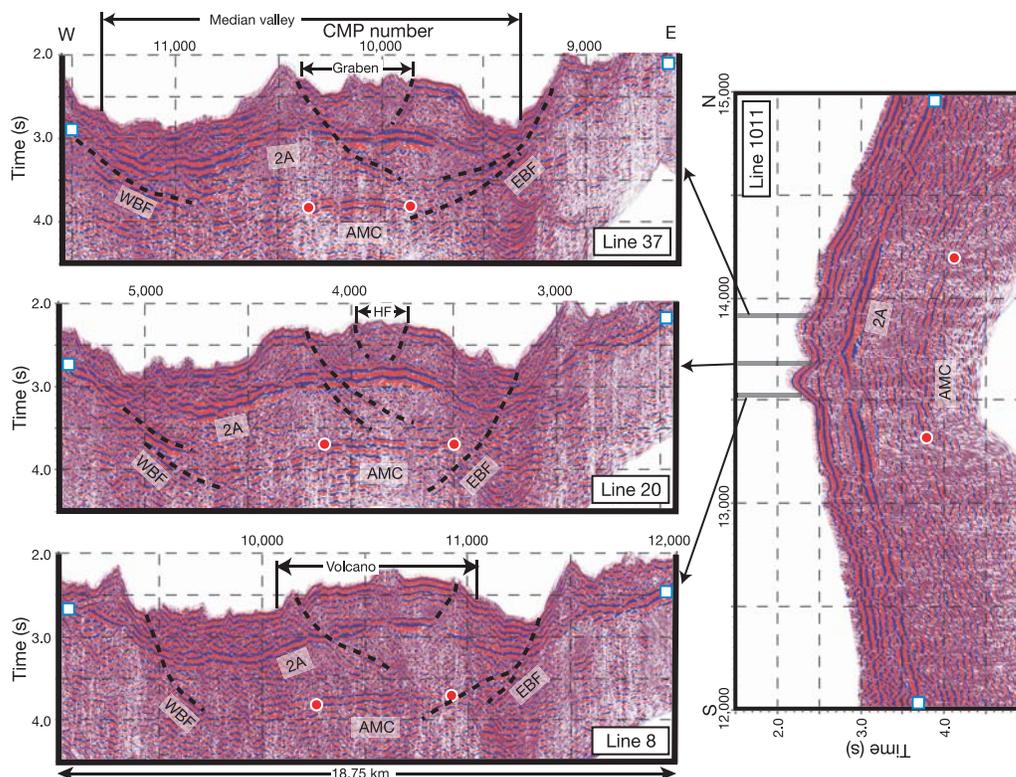

Figure 2 | Seismic reflection images of the AMC and faults. Seismic sections across the ridge axis (lines 8, 20 and 37) and along the ridge axis (line 1011). The vertical exaggeration is 1:1, assuming a velocity of 5 km s^{-1}. Blue and red ripples represent positive and negative trace amplitudes, respectively. Red circles show the limits of the AMC reflector, blue squares mark the layer 2A reflector and dashed black lines indicate principal faults (Supplementary Fig. S2 is without interpretive curves). Labels are placed just beneath the reflector to which they correspond. The AMC width decreases from the south (4 km) to the north (2.5 km) but the AMC continues for about 3 km north of the three-dimensional box (line 1011), beneath the graben. HF, hydrothermal vent field. CMP, common mid-point.
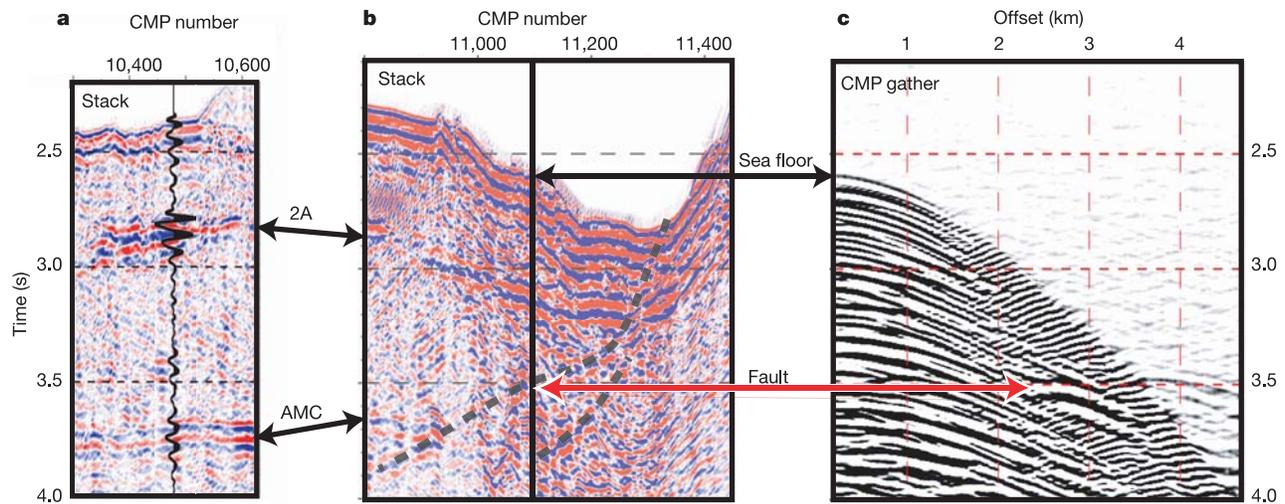
Figure 3 | Fault and AMC reflector details. Detailed seismic sections from line 8. **a**, Section showing the sea floor, layer 2A and the AMC reflector. The AMC reflector has the opposite polarity of the other reflectors. The black wiggle trace highlights the polarity of different events. **b**, The EBF, enlarged from Fig. 1. **c**, Super-CMP gather corresponding to the vertical black line in **b**, showing the fault reflection. This gather was obtained by combining six CMP and has been frequency-wavenumber (F-K) filtered to highlight the fault reflection.

geometry of the magma chamber, faults, and the seafloor features. Axial seismicity[21] and thermo-mechanical models of axial valley formation[22] suggest that isotherms corresponding to the brittle–ductile transition (500–700 °C) may lie as deep as 8 km below the sea floor at slow-spreading ridges. The presence of rift-bounding faults that seem to go down to at least 3–4 km depth suggests that the rift-forming tectonic processes (faulting) have coexisted with magmatism in the recent past. It is difficult to establish the age of the different structures, but it is certain that the graben bounding faults are younger than the volcano, because they cross-cut its otherwise unfaulted and smooth flanks. The synchronous presence of the AMC and deep penetrating faults suggests that there is a continuous interplay between magmatic and tectonic processes.

The discovery of the crustal magma chamber and deep penetrating faults also has important implications for the crustal accretion process at slow-spreading ridges. Thick crust beneath the volcano[9,14] may result from a robust melt supply at the centre of the segment where the crust is formed by cooling and crystallization of magma in crustal melt lenses[23], while lateral propagation of dykes over tens of kilometres could be responsible for crustal accretion towards the segment ends[24]. The neighbouring Azores hotspot could be responsible for higher melt production in the mantle, which could get focused at the centre of the segment, sustaining a long-lived magma

chamber in the crust. On the other hand, the overall morphology of the Lucky Strike segment with a well-developed axial valley suggests that the crust is largely cooled and brittle, and supports the idea that the imaged AMC might be the first direct evidence of melt at the roof of a short-lived crustal melt body. The composition of gabbros and overall lithospheric structure from slow-spreading ridges[25] does suggest that gabbros crystallize in intrusive bodies within a tectonically deforming crust and shallow mantle[26]. However, the high regional bathymetry, the presence of a large central volcano and a crustal AMC lead us to suggest that magmatism dominates the crustal accretion process at the Lucky Strike segment of the MAR.

It has been suggested that high-temperature seafloor hydrothermal activities at fast-spreading centres are linked to fresh melt supply in the crust[27]. The high-temperature hydrothermal vents observed on the Lucky Strike volcano also require a magmatic heat source, and we suggest that the AMC observed on the seismic profiles is this source. The axial valley bounding faults appear to penetrate down to AMC depth, so they may act as recharge pathways for hydrothermal circulation, allowing for sea water to penetrate efficiently down to near the AMC. Heated fluids would then flow vertically upwards in a narrow zone, forming the hydrothermal vent field[28].

Our results provide the first image, to our knowledge, of an axial magma chamber at a slow-spreading ridge segment, and its
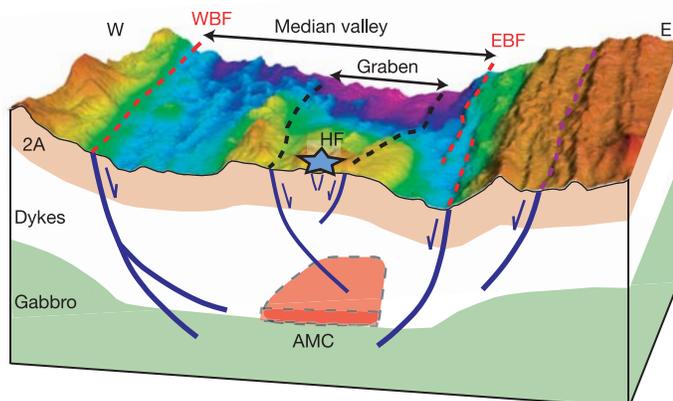

Figure 4 | Three-dimensional schematic view of the AMC and faults. Schematic diagram relating different features observed on seismic profiles to the bathymetry. Beneath the Lucky Strike volcano, layer 2A is about 1 km thick and a large AMC is present (up to 7 km long and 4 km wide). The median valley faults seem to continue down to and possibly beneath the AMC. The graben bounding faults terminate above the AMC in dykes and layer 2A.

interaction with active tectonic and hydrothermal processes. The along-axis extension of the magma chamber (<10 km) compared to the total segment length (~60 km) suggests a very efficient lateral dyke propagation away from the AMC, a length similar to that of dyking events at intermediate-spreading ridges[29]. Our results are also consistent with the presence of melt in the lower crust[20], and possible seismic reflectors that may be associated with melt bodies under the Snake Pit vent field[19]. We expect magma chambers to be common under long-lived hydrothermal fields at slow-spreading segments, particularly those within the rift valley, at or near the centre of segments, and hosted in basalt (such as Menez Gwen, Snake Pit[30]).

METHODS

Seismic reflection data were acquired using a 4.5-km-long digital streamer with 12.5-m receiver intervals towed at 15 m depth. The energy source was a 2,594 cubic inch 18-airgun array towed at a depth of about 12 m and tuned to provide a broadband (8–50 Hz) source with a strong first arrival. The record length was 11 s and the sample interval was 2 ms. A set of thirty-nine 18.75-km-long seismic reflection lines were spaced at 100 m apart and provided three-dimensional coverage in an 18.75×3.8 km^2 area. The shot interval was 37.5 m and the vessel speed was 4.5 knots. To obtain a high-resolution lateral image (6.25 m) across the ridge axis, lines were shot perpendicular to the ridge (109° azimuth). The along-axis line 1011 was shot at an interval of 75 m using a 5,638 cubic inch airgun array.

The seismic reflection data were quality controlled using nearly real-time onboard processing. The four lines (8, 20, 37, 1011) presented here were reprocessed assuming a two-dimensional geometry. The data were re-sampled to 4 ms and binned at 6.25 m spacing. A set of constant-velocity stacks was calculated to obtain stacking velocities for layer 2A and the AMC. The image quality is very sensitive to velocity so several tests were performed to optimize the velocity. Layer 2A stacked best at 1,900–2,100 m s^{-1}, whereas the AMC stacked at 3,000–3,300 m s^{-1}. A dipping reflector such as a fault requires higher stacking velocities. The median valley faults stacked best at a velocity of 3,000–4,000 km s^{-1}, depending upon the dip and depth. To relate images from one line to another and remove bias due to velocity model errors, we decided to use the same crustal velocities for all the lines: 1,900 m s^{-1} down to 600 ms beneath the sea floor and 3,100 m s^{-1} below that level. Slightly higher velocity does not influence the imaging of the sea floor because only near-offset data contribute to the stack as stretched large-offset data get muted (deleted) after normal moveout correction.

Seafloor scattering and multiples were the strongest noise in the data. To reduce the effect of multiples during migration, the seafloor multiples were muted. To remove the seafloor scattering, we used a frequency domain migration with a constant velocity of 1,500 m s^{-1}. Migration is sensitive to velocity, and therefore a constant velocity migration provided uniform and objective images. When interpreting these images, one should note that stacking flattens a dipping interface, and therefore after full crustal migration, a dipping event will get steeper and will map to a shallower depth.

There were several factors that facilitated the imaging of the magma chamber and faults. The fine lateral sampling (6.25 m), high fold (60) and the broadband source were essential. The line spacing of 100 m provided the along-axis continuity of the events. The noise due to seafloor scattering was reduced because of the smooth bathymetry over the Lucky Strike volcano and the presence of a wide median valley (12–15 km). The processing sequence used here was extremely valuable for preserving the lateral continuity of events along the line and correlation of events on different lines.

1. Cannat, M. Emplacement of mantle rocks in the seafloor at mid-ocean ridges. *J. Geophys. Res.* **98,** 4163–4172 (1993).
2. Collier, J. S. & Sinha, M. C. Seismic images of a magma chamber beneath the Lau Basin back-arc spreading centre. *Nature* **346,** 646–648 (1990).
3. Canales, J. P. et al. Upper crustal structure and axial topography at intermediate spreading ridges: Seismic constraints from the southern Juan de Fuca Ridge. *J. Geophys. Res.* **110,** B12104, doi:10.1029/2005/JB003630 (2005).
4. Detrick, R. S. et al. Multi-channel seismic imaging of a crustal magma chamber along the East Pacific Rise. *Nature* **326,** 35–41 (1987).
5. Kent, G. M. et al. Evidence from three-dimensional reflectivity images for enhanced melt supply beneath mid-ocean-ridge discontinuities. *Nature* **406,** 614–618 (2000).
6. Detrick, R. S., Mutter, J. C., Buhl, P. & Kim, I. I. No evidence from multichannel reflection data for a crustal magma chamber in the MARK area on the Mid-Atlantic Ridge. *Nature* **347,** 61–64 (1990).
7. Calvert, A. J. Backscattered coherence noise and seismic reflection imaging of the oceanic crust: An example from the rift valley of Mid-Atlantic Ridge at 23°N. *J. Geophys. Res.* **102,** 5119–5133 (1997).
8. Navin, D. A., Peirce, C. & Sinha, M. C. The RAMESSES experiment—II. Evidence for accumulated melt beneath a slow spreading ridge from wide-angle refraction and multichannel reflection profiles. *Geophys. J. Int.* **135,** 746–772 (1998).
9. Cannat, M. et al. Mid-Atlantic ridge—Azores hotspot interactions: Along-axis migration of a hotspot-derived magmatic pulse 14 to 4 ma ago. *Earth Planet. Sci. Lett.* **173,** 257–269 (1999).
10. Dosso, L. et al. The age and distribution of mantle heterogeneity along the Mid-Atlantic ridge (31–41°N). *Earth Planet. Sci. Lett.* **170,** 269–286 (1999).
11. Schilling, J.-G. Fluxes and excess temperatures of mantle plumes inferred from their interaction with migrating mid-ocean ridges. *Nature* **352,** 397–403 (1991).
12. Detrick, R. S., Needham, H. D. & Renard, V. Gravity anomalies and crustal thickness variations along the Mid-Atlantic Ridge between 33°N and 40°N. *J. Geophys. Res.* **100,** 3767–3787 (1995).
13. Dziak, R. P. et al. Evidence of a recent magma dike intrusion at the slow spreading Lucky Strike segment, Mid-Atlantic Ridge. *J. Geophys. Res.* **109,** B12102, doi:12110.11029/12004JB003141 (2004).
14. Escartín, J., Cannat, M., Pouliquen, G., Rabain, A. & Lin, J. Crustal thickness of V-shaped ridges south of the Azores; interaction of the Mid-Atlantic Ridge (36°-39° N) and the Azores hotspot. *J. Geophys. Res.* **106,** 21719–21735 (2001).
15. Humphris, S. E., Fornari, D. J., Scheirer, D. S., German, C. R. & Parson, L. M. Geotectonic setting of hydrothermal activity on the summit of Lucky Strike seamount (37°17′N, Mid-Atlantic Ridge). *Geochem. Geophys. Geosyst.* **3,** doi:10.1029/2001GC000284 (2002).
16. Langmuir, C. et al. Hydrothermal vents near a mantle hotspot: the Lucky Strike vent field at 37°N on the Mid-Atlantic Ridge. *Earth Planet. Sci. Lett.* **148,** 69–91 (1997).
17. Desbruyères, D. et al. Variations in deep-sea hydrothermal vent communities on the Mid-Atlantic Ridge near the Azores plateau. *Deep-Sea Res.* **48,** 1325–1346 (2001).
18. Thatcher, W. & Hill, D. P. A simple model for the fault-generated morphology of slow-spreading mid-ocean ridges. *J. Geophys. Res.* **100,** 561–570 (1995).
19. Calvert, A. J. Seismic evidence for a magma chamber beneath the slow-spreading Mid-Atlantic Ridge. *Nature* **377,** 410–414 (1995).
20. Canales, J. P., Collins, J. A., Escartin, J. & Detrick, R. S. Seismic structure across the rift valley of the Mid-Atlantic ridge at 23°20′N (MARK area): Implications for crustal accretion processes at slow-spreading ridges. *J. Geophys. Res.* **105,** 28411–28425 (2000).
21. Toomey, D. R., Purdy, G. M. & Solomon, S. C. Micro-earthquakes beneath the median valley of the Mid-Atlantic ridge near 23°N: tomography and tectonics. *J. Geophys. Res.* **93,** 9093–9112 (1988).
22. Chen, Y. & Morgan, W. J. Rift valley/no rift valley transition at mid-ocean ridges. *J. Geophys. Res.* **95,** 17571–17581 (1990).
23. Maclennan, J. A., Hulme, T. & Singh, S. C. Thermal models of oceanic crustal accretion: Linking geophysical, geological and petrological observations. *Geochem. Geophys. Geosyst.* **5,** doi:10.1029/2003GC000605 (2003).
24. Smith, D. K. & Cann, J. R. Constructing the upper crust of the Mid-Atlantic Ridge; a reinterpretation based on the Puna Ridge, Kilauea volcano. *J. Geophys. Res.* **104,** 25379–25399 (1999).
25. Meurer, W. P. & Gee, J. S. Evidence for the protracted construction of slow-spread oceanic crust by small magmatic injections. *Earth Planet. Sci. Lett.* **201,** 45–55 (2002).
26. Cannat, M. How thick is the magmatic crust at slow spreading oceanic ridges? *J. Geophys. Res.* **101,** 2847–2857 (1996).
27. Singh, S. C., Kent, G. M., Collier, J. S., Harding, A. J. & Orcutt, J. A. Melt to mush variations in crustal magma properties along the ridge crest at the southern East Pacific Rise. *Nature* **394,** 874–878 (1998).
28. Wilcock, W. S. D. & Delaney, J. R. Mid-ocean ridge sulphide deposits: Evidence for heat extraction from magma chambers or cracking fronts? *Earth Planet. Sci. Lett.* **145,** 49–64 (1996).
29. Dziak, R. P. & Fox, C. G. Long-term seismicity and ground deformation at Axial Volcano, Juan de Fuca Ridge. *Geophys. Res. Lett.* **26,** 3641–3644 (1999).
30. Von Damm, K. L. in *Seafloor Hydrothermal Systems* (eds Humphris, S. E. et al.) 222–247 (Geophysical Monograph 91, American Geophysical Union (AGU), Washington DC, 1995).